

Structural Phase Transition Driven by Spin–Lattice Interaction in a Quasi-One-Dimensional Spin System of [1-(4'-Iodobenzyl)pyridinium][Ni(mnt)₂]

X. M. Ren,^{*,†} T. Akutagawa,[†] S. Nishihara,[‡] T. Nakamura,^{*,†} W. Fujita,[§] and K. Awaga[‡]

Research Institute for Electronic Science, Hokkaido University, Sapporo 060-0812, Japan, and CREST, Japan Science and Technology Corporation (JST), Kawaguchi 332-0012, Japan, Department of Chemistry, Graduate School of Science, Nagoya University, Chikusa-ku, Nagoya 464-8602, Japan, and Research Center of Materials Science, Nagoya University, Chikusa-ku, Nagoya, 464-8602, Japan

Received: April 18, 2005; In Final Form: July 7, 2005

Crystal structures and magnetic properties were determined for two novel compounds, [1-(4'-iodobenzyl)pyridinium][M(mnt)₂] (mnt²⁻ = maleonitriledithiolate; M = Ni (**1**) or Cu (**2**)). At room temperature, single crystals of **1** and **2** were isostructural, featuring the formation of segregated columnar structures with regular stacks of cations and anions. For crystal **1**, a magnetic transition was observed at ~120 K; furthermore, its magnetic behavior was consistent with that of a regular Heisenberg antiferromagnetic (AFM) chain of $S = 1/2$ in the high-temperature phase (HT phase) and that of a spin-gap system in the low-temperature phase (LT phase). Such a phenomenon is similar to the spin-Peierls transition. However, the crystal structure of **1** in the LT phase at 100 K revealed that its structural transition is associated with the magnetic transition. Because crystal **2** ($S = 0$) did not exhibit a structural transition, the structural transition of **1** is driven by spin–lattice interaction.

Introduction

Crystalline materials that possess switch property and memory transduction have a great potential to be used in molecular spin-electronic or “spintronic” devices, such as next-generation sensors, molecular switches, and memory devices.^{1–3} One of the most spectacular examples of such materials is the spin-crossover compound, in which a molecular species containing an octahedrally coordinated transition metal ion with a $3d^n$ ($n = 4–7$) electronic configuration exhibits a crossover between a low-spin state and a high-spin state under external perturbations (change of temperature, application of pressure, light irradiation, or pulsed magnetic field).^{3,4} Another molecular system that has demonstrated a spin-switch property is that of a radical compound with a quasi-one-dimensional (quasi-1D) stacking structure. In such a compound, the magnetic interactions within a stack are governed by the intermolecular π orbital overlap as well as the spin-polarization effect; thus, the property of the magnetic exchange is sensitive to the intermolecular contacts; upon application of an external perturbation (that causes a change in the intermolecular contacts), the spin transition presumably occurs.^{2,5,6}

Our studies have focused on the design, preparation, and investigation of a novel spin-transition molecular system that is based on the molecular architecture of [M(mnt)₂]⁻ (mnt²⁻ = maleonitriledithiolate; M = Ni, Pd, or Pt). The formation of columnar stacks is favorable because such molecules possess (1) a flat molecular and extended electronic structure and (2) intermolecular interactions between [M(mnt)₂]⁻ anions, such as

π – π stacking, $S \cdots S$, or $S \cdots M$ interactions. The magnetic exchange characteristic is highly sensitive to the intermolecular contacts and the overlap pattern between neighboring anions. For example, in the case of adjacent anions of the [M(mnt)₂]⁻ overlap in a slipped M-over-S configuration, the spin-polarization effect between the large positive spin densities on the M ions and the small negative spin densities on the S atoms of the adjacent anions of [M(mnt)₂]⁻ may lead to a ferromagnetic (FM) interaction; in contrast, direct contacts between $S \cdots S$ or $M \cdots M$ may result in an antiferromagnetic (AFM) interaction⁶ that an external perturbation could trigger a spin transition. Accordingly, a key issue in our research is the control of the [M(mnt)₂]⁻ anions during the columnar arrangement. Because the stacking pattern of the [M(mnt)₂]⁻ anions strongly depends on the molecular topology of the counteranion, we proposed that the formation of a quasi-one-dimensional magnet of [M(mnt)₂]⁻ was attainable by modifying the molecular structure of the counteranion. Derivatives of benzylpyridinium ([RBzPy]⁺) can serve as flexible cations that can be adjusted via modifying the nature of the groups on the aromatic rings.^{7,8} Consequently, we have recently prepared a series of [RBzPy][M(mnt)₂] ion-pair compounds (the substituent groups of the cation and the metal ions of the anion are listed in Table 1) that form a structure with segregated stacks of cation and anion and show a spin-Peierls-like transition.⁹ Unfortunately, some interesting features of this series of compounds remain poorly understood; for example, although all compounds are isostructural at room temperature (the anionic stack is regular in the high-temperature (HT) phase), magnetostructural transition was observed for some compounds, whereas only magnetic transition, for others. To investigate this puzzling phenomenon, we have carried out the design, synthesis, and structural characterization of a series of compounds that do not possess a spin.

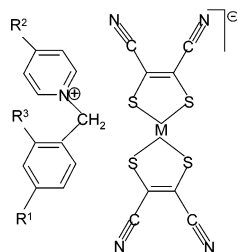
Herein, we report on two ion-pair compounds [IPyBz][M(mnt)₂] (IPyBz⁺ = 1-(4'-iodobenzyl)pyridinium; M = Ni or

* To whom correspondence should be addressed. Phone: +81 11-706-2849. Fax: +81 11-706-4972. E-mail: xmren@es.hokudai.ac.jp (X.M.R.); tnaka@imd.es.hokudai.ac.jp (T.N.).

[†] Hokkaido University and Japan Science and Technology Corporation (JST).

[‡] Graduate School of Science, Nagoya University.

[§] Research Center of Materials Science, Nagoya University.

TABLE 1: Reported Compounds in the Series of [R¹R²R³BzPy][M(mnt)₂] that Exhibit a Magnetic Transition

R1	R2	R3	M	reference
I	H	H	Ni	present paper
NO ₂ , Cl, Br	H	H	Ni	8a
F	H	H	Ni	8b
CN	H	H	Ni	8c
NO ₂ , Cl, Br	H	H	Pt	8d
Br	H	F	Ni	8e
Br	NH ₂	H	Ni	8f
CN	NH ₂	H	Ni	8g
Cl	NH ₂	H	Ni	8h
vinyl	H	H	Ni	8i

Cu). The crystals of these two compounds are isostructural with each other at room temperature, in which the segregated stacks of cations and anions are regular. The [Ni(mnt)₂][−] compound formed a one-dimensional regular AFM chain system with $S = 1/2$, which exhibited an abrupt drop in magnetic susceptibility (a spin-Peierls-like transition) below ~ 120 K, whereas the [Cu(mnt)₂][−] compound (without spin) did not show a structural transition.

Experimental Section

Preparation of Compounds. Na₂mnt, [IPyBz]Br,⁷ and [IPyBz]₂[M(mnt)₂] (M = Ni or Cu) were prepared according to published procedures.¹⁰

[IPyBz][Ni(mnt)₂] (1). To a solution of [IPyBz]₂[Ni(mnt)₂] (932 mg, 1.0 mmol) in acetonitrile (5 mL) was added I₂ (150 mg, 0.6 mmol) and methanol (30 mL). The mixture was stirred for 10 min and then placed in a refrigerator at 4 °C for 24 h. The resulting brown microcrystalline was collected by filtration, washed with methanol, and dried under vacuum (yield: 520 mg, 82%). Single crystals suitable for X-ray structure analysis were obtained by diffusing diethyl ether into an acetonitrile solution of **1**. Elemental analysis: Calcd for C₂₀H₁₁N₅S₄INi: C, 37.8; H, 1.75; N, 11.0%. Found: C, 37.9; H, 1.91; N, 10.9%.

[IPyBz][Cu(mnt)₂] (2). The procedure as described above for **1**, but with [1-(4'-iodobenzyl)pyridinium]₂[Cu(mnt)₂] as the starting material, was followed to afford **2** (yield: 442 mg, 69%). Single crystals suitable for X-ray structure analysis were grown by slowly cooling an acetonitrile solution of **2**. Elemental analysis: Calcd for C₂₀H₁₁N₅S₄ICu: C, 37.5; H, 1.73; N, 10.9%. Found: C, 37.3; H, 1.75; N, 10.6%.

Magnetic Susceptibility and Heat Capacity Measurements. Magnetic susceptibility measurements for polycrystalline samples over the range 2–350 K and for a crystal with dimensions of 3.0 × 1.0 × 0.2 mm³ and a mass of 0.40 mg over the range 2–300 K were carried out using a Quantum Design MPMS-XL superconducting quantum interference device (SQUID) magnetometer under 1.0 T. Heat capacity measurements were performed following the relaxation method using a Quantum Design Physical Property Measurement System (PPMS) over the range 2–150 K on both heating and cooling processes. A crystal with dimensions of 3.0 × 1.0 × 0.2 mm³ and a mass of 0.40 mg was attached to the sample platform with a small amount of grease.

X-ray Structural Analyses. Crystallographic data were collected using a Rigaku Raxis-Rapid diffractometer with Mo K α ($\lambda = 0.71073$ Å) radiation from a graphite monochromator. Structure refinements were performed using the full-matrix least-squares method on F^2 . Calculations were performed using SHELXL-97 software packages.¹¹ Parameters were refined using anisotropic temperature factors, with the exception of those for the hydrogen atom. The hydrogen atoms were introduced at calculated positions. Details of the crystal parameters, data collection, and refinement for **1** and **2** at 293 and 100 K are summarized in Table 2. The bond lengths for the [M(mnt)₂][−] (M = Ni or Cu) anions, along with their estimated standard deviations, are listed in Supporting Information Table S1. Some important intermolecular distances are listed in Table 3. The determination of the crystal structure of **1** at low temperatures (below ~ 140 K) was further complicated by the inaccuracy of the data due to diffuse scattering that is driven by magnetoelastic interactions. To minimize the effect of diffuse scattering, the diffraction intensities of **1** at 100 K were obtained using a reduced exposure time of 40 s. Although the crystal structure was consequently solved and refined, parameters such as wR_2 and R_1 remained somewhat high. Nonetheless, the main difference in the structures of the HT and low-temperature (LT) phases was undoubtedly in accordance with the crystal data analyses.

TABLE 2: Crystallographic Data for 1 and 2^a

	1 (293 K)	1 (100 K)	2 (293 K)	2 (100 K)
molecular formula	C ₂₀ H ₁₁ IN ₅ NiS ₄	C ₂₀ H ₁₁ IN ₅ NiS ₄	C ₂₀ H ₁₁ IN ₅ CuS ₄	C ₂₀ H ₁₁ IN ₅ CuS ₄
CCDC no.	CCDC-260866	CCDC-260867	CCDC-260868	CCDC-260869
Mr	635.18	635.18	640.03	640.03
space group	$P2_1/a$	$P\bar{1}$	$P2_1/a$	$P2_1/a$
$a/\text{Å}$	7.6048(15)	7.387(3)	7.625(1)	7.473(2)
$b/\text{Å}$	26.742(5)	26.18(1)	26.524(6)	26.373(9)
$c/\text{Å}$	12.057(2)	11.886(8)	11.984(3)	11.883(4)
α/deg	90	88.57(2)	90	90
β/deg	102.727(3) ^o	77.28(2)	102.614(9)	102.34(1)
γ/deg	90	87.29(2)	90	90
$V/\text{Å}^3$	2391.8(8)	2239(2)	2365.3(8)	2287(1)
Z	4	4	4	4
μ/mm^{-1}	2.469	2.637	2.600	2.688
$\lambda/\text{Å}$	0.71073	0.71073	0.71073	0.71073
$\rho/\text{g cm}^{-3}$	1.764	1.884	1.797	1.858
R_1	0.0471	0.248	0.039	0.028
wR_2	0.1144	0.559	0.128	0.074

^a $R_1 = \sum(|F_0| - |F_c|)/\sum|F_0|$, $wR_2 = \sum w(|F_0|^2 - |F_c|^2)^2/\sum w(|F_0|^2)^{1/2}$.

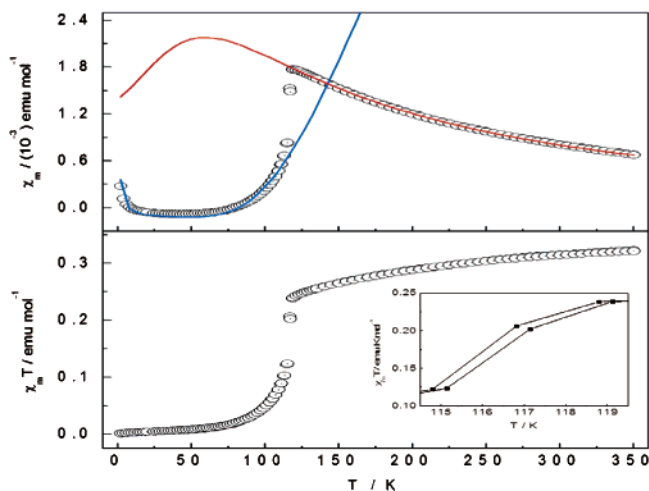


Figure 1. Plots of χ_m and $\chi_m T$ vs T of a polycrystalline sample of **1**. (upper) Open circles represent experimental data; the solid lines represent the best fit data. (bottom) Plot of $\chi_m T$ reproduced by subtracting the contributions of diamagnetism and possible van Vleck paramagnetism (see text).

TABLE 3: Intermolecular and Interplane Distances (\AA) in Both the HT and LT Phases

	1 (293 K)	1 (100 K)	2 (293 K)	2 (100 K)
d_1	3.981	3.719	4.004	3.913
d_2	3.981	3.889	4.004	3.913
h_1	3.602	3.512	3.578	3.499
h_2	3.635	3.518	3.582	3.450
c_1	4.598	4.393	4.579	4.489
c_2	4.598	4.535	4.579	4.489
g_1	3.699	3.574	3.714	3.636
g_2	3.885	3.793	3.898	3.826

Details about Molecular Orbital Calculations. Extended Hückel molecular orbital calculations^{12a} were carried out using the CAESAR2 and SAMOA program packages.^{12b} Double- ζ Slater-type orbitals¹³ were used for the C, N, and S atoms as well as for the Ni 3d orbitals.

Results and Discussion

Magnetic Susceptibilities. The temperature dependence of the magnetic susceptibility (χ_m) for polycrystalline **1** is displayed in Figure 1. The value of $\chi_m T$ per mole of **1** at 350 K is $0.322 \text{ emu}\cdot\text{K}\cdot\text{mol}^{-1}$, which is slightly lower than the expected value for an independent spin of $S = 1/2$. The initial smooth decrease of the $\chi_m T$ values, with cooling temperatures, is indicative of antiferromagnetic exchange interactions between the nearest neighboring spins. The abrupt drop of the $\chi_m T$ value at ~ 120 K implies the occurrence of a magnetic transition. The subsequent drop to zero at around 90 K indicates that **1** is nearly diamagnetic below 90 K. When the temperature was increased from 2 to 350 K, a very small hysteresis loop (less than 1 K) was detected, as illustrated in the inset of Figure 1. Temperature dependences of the magnetic susceptibility of a single crystal at 1.0 T parallel to the a - and c -axes (cf. Supporting Information Figure S1) nearly coincided with each other but parallel to the b -axis exhibited small differences from the other two cases.

Crystal Structures. Because **1** and **2** are isostructural at 293 K, only the detailed structure of **1** is presented. The asymmetric unit within a cell that is comprised of a coupled $[\text{Ni}(\text{mnt})_2]^-$ anion and IPyBz^+ cation of **1** is shown in Figure 2a. Most of the bond lengths and angles are in good agreement with those

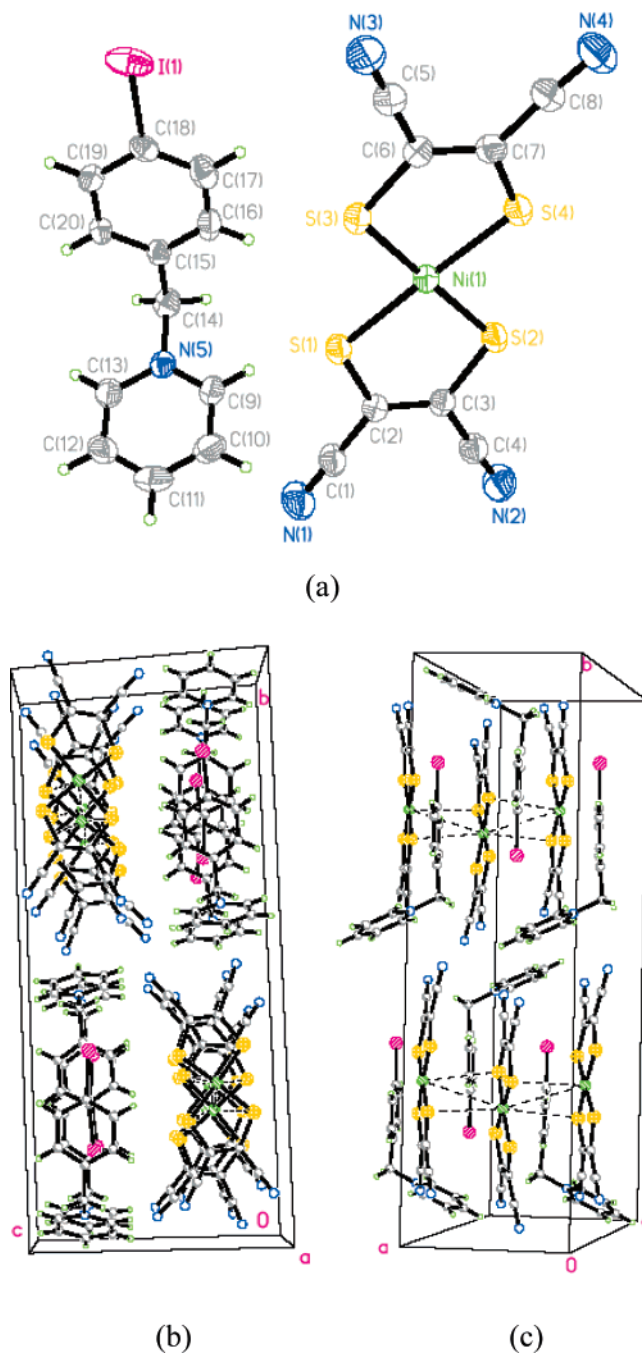


Figure 2. (a) Molecular structure of **1** and the segregated stacks of cations and anions along the a -axis; (b) top view; (c) side view.

of various $[\text{Ni}(\text{mnt})_2]^-$ compounds.⁹ Both the anions and the cations constructed segregated stacks that were parallel to the a -axis (Figure 2b and c). Within an anionic stack, the face-to-face anions slid along the b -axis, to eclipse each other. The distances between the $[\text{Ni}(\text{mnt})_2]^-$ molecular planes, which are defined by the Ni ion and four coordinated S atoms, are $h_1 = 3.602 \text{ \AA}$ and $h_2 = 3.635 \text{ \AA}$ (Figure 3a), while the adjacent $\text{Ni}\cdots\text{Ni}$ distances are identical ($d_1 = d_2 = 3.981 \text{ \AA}$), even if the atoms lie on a general point position (cf. note 14). Within a cationic stack, the neighboring cations overlap in a boat conformation, as illustrated in Figure 3b. The central-to-central distances of the adjacent benzene rings are $c_1 = c_2 = 4.598 \text{ \AA}$, and the corresponding interplanar spaces are $g_1 = 3.699$ and $g_2 = 3.885 \text{ \AA}$.

In crystal **2**, the $[\text{Cu}(\text{mnt})_2]^-$ anions and the IPyBz^+ cations are stacked in columns that are similar to those in **1**. The bond

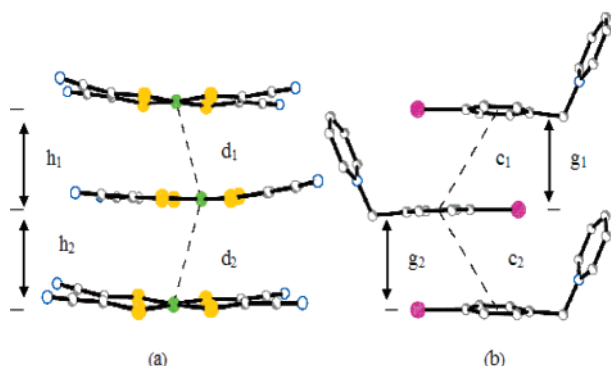


Figure 3. Separations (Å) between neighboring ions within (a) an anionic stack and (b) a cationic stack.

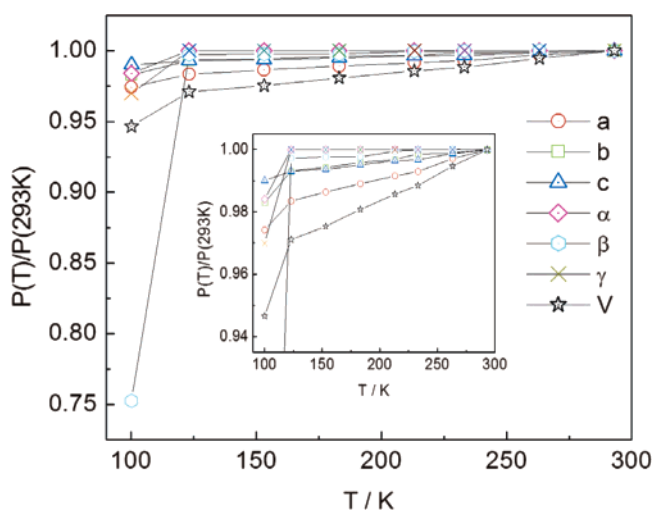


Figure 4. Temperature dependence of the relative cell parameters of **1**, which is defined as $P(T)/P(293\text{ K})$, where $P(T)$ represents the lattice parameters at T K.

lengths and angles for the $[\text{Cu}(\text{mnt})_2]^-$ anion are in good agreement with those for $[\text{TBA}][\text{Cu}(\text{mnt})_2]^{15}$ (summarized in Supporting Information Table S1). To highlight the comparisons to **1**, important intermolecular distances are listed in Table 3 and illustrated in Figure 3; these include c_1 and c_2 (center-to-center distances of neighboring benzene rings), d_1 and d_2 (distances of intermetal ions in an anionic stack), g_1 and g_2 (interplanar distances between neighboring benzene rings), and h_1 and h_2 (interplanar distances between the mean plane defined by the M ion and coordinated S atoms).

For **1**, the space group decreases from $P2(1)/a$ in the HT phase to $P\bar{1}$ in the LT phase at 100 K.¹⁵ Moreover, the asymmetric unit switches from a IPyBz^+ and $[\text{Ni}(\text{mnt})_2]^-$ pair in the HT phase into two ion pairs in the LT phase. Although the molecular structures are nearly identical, distinct differences were observed between the stacking structures in the LT and HT phases. At the phase transition, nonuniform compression and slippage of both the cation and the anion stacks cause (1) alternating distances of the adjacent $\text{Ni}\cdots\text{Ni}$ in an anionic stack ($d_1 = 3.719\text{ \AA}$ and $d_2 = 3.889\text{ \AA}$) and (2) distortion within a cationic stack as reflected in the central-to-central separations between adjacent benzene rings ($g_1 = 4.393\text{ \AA}$ and $g_2 = 4.535\text{ \AA}$). The temperature dependences of the relative lattice parameters, which are defined as $P_{\text{cell}}(T)/P_{\text{cell}}(293\text{ K})$, where $P_{\text{cell}}(T)$ and $P_{\text{cell}}(293\text{ K})$ represent the cell parameters at T and 293 K, respectively, are depicted in Figure 4. Upon cooling to 120 K, all parameters decrease smoothly without any significant

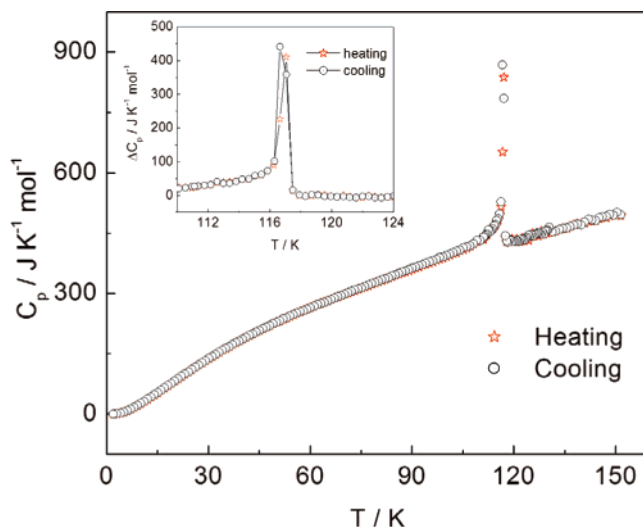


Figure 5. Temperature dependence of the molar heat capacity of **1**. The open stars and circles represent data in heating and cooling processes, respectively. The inset shows the excess heat capacity around the phase transition temperature.

discontinuous change; below 120 K, however, a sharp drop is observed, thus indicating the existence of a structural transition in **1**.

Except for the shorter intermolecular distances at the lower temperature, the molecular and stacking structures for crystal **2** at 100 and 293 K were nearly identical. In contrast to **1**, however, uniform compression upon cooling was observed; specifically, the $\text{Cu}\cdots\text{Cu}$ distance between adjacent anions in a stack and the central-to-central distance between adjacent benzene rings remained unchanged (Supporting Information Table S1), thus implying that a structural transition does not occur for **2**.

Heat Capacity. The results of the heat capacity measurements for **1** are shown in Figure 5. A sharp thermal abnormality with λ shape was observed at $\sim 120\text{ K}$. Although the $C_p(T)-T$ plots in the heating and cooling procedures are superimposable, a small but significant supercooling/heating phenomenon (less than 1 K), which coincided with the small hysteresis loop in the susceptibility measurements, was observed. Furthermore, the peak temperature at 117 K in the heating procedure coincides with the temperature at which the abrupt drop of magnetic susceptibility occurs. The transition in **1**, therefore, is not a spin-Peierls transition.

In the first-order approximation, a normal heat capacity would appear as a smooth curve.¹⁶ Upon subtraction of the contribution of such a normal heat capacity, the excess heat capacity around the transition is displayed in the inset of Figure 5. The entropy of this transition (which includes the contribution of both structural and spin) is estimated as $4.34\text{ J}\cdot\text{K}^{-1}\cdot\text{mol}^{-1}$. Because this value is lower than the theoretical maximum of spin entropy for a mole of $S = 1/2$ ion ($R \ln 2 \approx 5.76\text{ J}\cdot\text{K}^{-1}\cdot\text{mol}^{-1}$),¹⁷ it can be suggested that a substantial short-range order persists over the temperature of the transition of **1**. The short-range order is an indication of a lowered dimensionality of the magnetic spin system and is consistent with the chain structure of the $[\text{Ni}(\text{mnt})_2]^-$ anions in crystal **1**.¹⁸

Structurally, crystal **1** should exist as a nearly perfect 1D spin system because the anionic stacks are separated by the diamagnetic cationic stacks. Magnetic interactions between the anionic stacks, therefore, should be significantly less than that within an anionic stack. Qualitative theoretical analyses of the magnetic exchange interactions between the nearest spins in both the HT

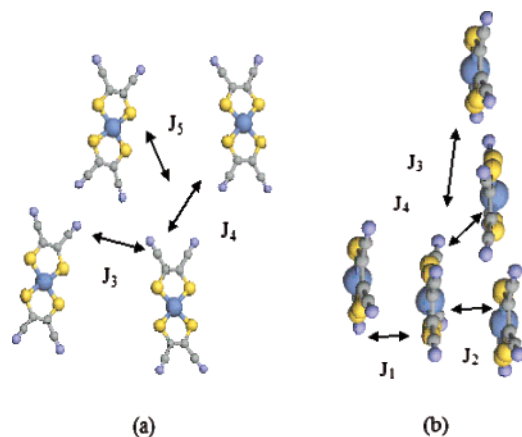


Figure 6. Schematic (a) top and (b) side views of the spin dimers in crystal **1**. J_1 and J_2 represent magnetic exchange interaction within a stack, whereas J_3 , J_4 , and J_5 represent those between stacks.

TABLE 4: Values of $(\Delta e)^2$ ^a and Ni^b · · Ni^b Distances of Various Spin-Exchange Paths at 293 and 100 K for **1, Where the Spin Dimers Were Identified by Specifying Their Ni^b · · Ni Distances**

spin dimer	293 K		100 K	
	distance	$(\Delta e)^2$	distance	$(\Delta e)^2$
	(a) Intrastack			
J_1	3.981	8226	3.719	450644
J_2	3.981	8226	3.889	21228
	(b) Interstack			
J_3	11.876	0	11.654	2025
J_4	15.038	0	14.808	2025
J_5	14.617	0	14.433	2025

^a In units of (meV)². ^b In units of Å.

and LT phases were carried out using the extended Hückel molecular orbital calculation.¹² With respect to a spin system with AFM exchange interaction, the magnetic exchange energy (J_{AF}) between two spin sites (spin dimer) is described as

$$J_{AF} \propto -\frac{(\Delta e)^2}{U_{\text{eff}}} \quad (1)$$

where the spin-orbital interaction energy (Δe) is defined as the energy split between the two magnetic orbitals of a $[\text{Ni}(\text{mnt})_2]^{2-}$ spin dimer and U_{eff} is the effective on-site repulsive energy (nearly constant for a defined magnetic solid). Therefore, J_{AF} can be estimated with reasonable accuracy using the corresponding $(\Delta e)^2$.^{19,20} Spin interactions between adjacent spins in both the HT and LT phases are schematically illustrated in Figure 6. The results of the calculations are presented in Table 4. The values of $(\Delta e)^2$ show that the magnetic interactions of J_1 and J_2 within a stack are identical, whereas those of J_3 , J_4 , and J_5 between the stacks are zero in the HT phase. In the latter three cases, the corresponding highest occupied molecular orbital (HOMO) exists as a 2-fold degeneracy. Therefore, magnetic interactions do not exist between two spin sites, and the energy split between the two magnetic orbitals is zero. These results demonstrate that this spin system is a perfectly regular one-dimensional AFM chain in the HT phase. Within a stack in the LT phase, however, the regular magnetic chain in the HT phase is distorted to yield unequal values of J_1 and J_2 . Moreover, finite magnetic interaction between stacks was observed. The magnetic behavior of **1** in the HT phase is approximately described as that of a uniform Heisenberg linear chain system. Magnetic susceptibility in the HT phase was simulated by a regular

Heisenberg model of linear chain with $S = 1/2$ ²¹ using

$$\chi_m = \frac{Ng^2\mu_B^2}{k_B T} \frac{A + BX^{-1} + CX^{-2}}{1 + DX^{-1} + EX^{-2} + FX^{-3}} + \chi_0 \quad (2)$$

where $X = k_B T/|J|$, in which J is the magnetic exchange constant of the neighboring spins in a magnetic chain, the coefficients $A-F$ in the power series are $A = 0.25$, $B = 0.149\ 95$, $C = 0.300\ 94$, $D = 1.9862$, $E = 0.688\ 54$, and $F = 6.0626$, and χ_0 represents the sum of the diamagnetic and the Van Vleck paramagnetic components. The best fit to eq 2 resulted in $|J|/k_B = 46.0$ K and $\chi_0 = -2.6 \times 10^{-4}$ emu·mol⁻¹ with a fixed value of $g = 2.017$.²² Because the magnetic susceptibility exhibited a spin-gap feature in the LT phase, best fit calculations were carried out using²³

$$\chi_m = \frac{\alpha}{T} \exp(-\Delta/T) + \frac{C}{T} + \chi_0 \quad (3)$$

where the fitting parameters are $\alpha = 17.2$ emu·K⁻¹·mol⁻¹, $\Delta = 606.2$ K, $C = 1.0 \times 10^{-3}$ emu·K·mol⁻¹, and $\chi_0 = -1.4 \times 10^{-4}$ emu·mol⁻¹.

The observed phenomena in **1** are very similar to that of a spin-Peierls transition. However, evidence obtained from the crystal structure analyses in the HT and LT phases as well as the temperature dependence of the lattice parameters clearly demonstrate that the transition is that of a magnetostructural type. In contrast, crystal **2**, which is isostructural with **1** and is diamagnetic, does not exhibit a structural transition over the same temperature region. These observations imply that spin-lattice interactions play an important role in the structural transition of **1** and that the structure transition of **1** is driven by spin-lattice interactions.

Conclusion and Remarks

Investigations were carried out to study a peculiar magnetic transition for $[\text{IPyBz}][\text{Ni}(\text{mnt})_2]$ (**1**), which is typically a regular Heisenberg AFM linear chain in the HT phase but opens a spin gap in the LT phase. Such behavior is similar to that of a spin-Peierls transition. A sharp thermal anomaly with a λ shape, which corresponded with this transition in C_p measurements, indicated the transition is a first-order one. A supercooling/heating phenomenon consisting of a small hysteresis loop (less than 1 K) was observed in magnetic susceptibility measurements. Crystal structural analyses, above and below the transition, as well as the temperature dependence of the cell parameters revealed that the transition is that of a magnetostructural type. In contrast, a structural transition was not observed for **2**, which is diamagnetic and isostructural with **1** at room temperature. These results indicate that the structural transition in **1** is driven by spin-lattice interactions.

Acknowledgment. This work was partly supported by a Grant-in-Aid for Science Research from the Ministry of Education, Culture, Sports, Science and Technology of Japan. The authors thank Prof. Nomura and Dr. Ichimura for the use of the SQUID magnetometer. X.M.R., a JSPS fellow (ID no. P03271), thanks the Japan Society for the Promotion of Science for financial support.

Supporting Information Available: Tables of the bonding distances for the anionic moieties of **1** and **2**, plots of $\chi_m(T)-T$ of a single-crystal sample of **1** and a polycrystalline sample of **2**, and X-ray crystallographic files (CIF) of **1** and **2** in both the HT and LT phases. This material is available free of charge via the Internet at <http://pubs.acs.org>.

References and Notes

- (1) (a) Migliori, J. M.; Reiff, W. M.; Arif, A. M.; Miller, J. S. *Inorg. Chem.* **2004**, *43*, 6875. (b) Brusso, J. L.; Clements, O. P.; Haddon, R. C.; Itkis, M. E.; Leitch, A. A.; Oakley, R. T.; Reed, R. W.; Richardson, J. F. *J. Am. Chem. Soc.* **2004**, *126*, 8256. (c) Letard, J. F.; Guionneau, P.; Goux-Capes, L. *Top. Curr. Chem.* **2004**, *235*, 221. (d) Galet, A.; Niel, V.; Muñoz, M. C.; Real, J. A. *J. Am. Chem. Soc.* **2003**, *125*, 14224. (e) Itkis, M. E.; Chi, X.; Cordes, A. W.; Haddon, R. C. *Science* **2002**, *296*, 1443.
- (2) Fujita, W.; Awaga, K. *Science* **1999**, *286*, 261.
- (3) Kahn, O.; Martinez, C. J. *Science* **1998**, *279*, 44.
- (4) (a) Reger, D. L.; Gardinier, J. R.; Gemmill, W. R.; Smith, M. D.; Shahin, A. M.; Long, G. J.; Rebbouh, L.; Grandjean, F. *J. Am. Chem. Soc.* **2005**, *127*, 2303. (b) Dorbes, S.; Valade, L.; Real, J. A.; Faulmann, C. *Chem. Commun.* **2005**, 69. (c) Fujigaya, T.; Jiang, D. L.; Aida, T. *J. Am. Chem. Soc.* **2003**, *125*, 14690. (d) König, E. *Struct. Bonding (Berlin)* **1991**, *76*, 51. (e) Gütllich, P. *Struct. Bonding (Berlin)* **1981**, *44*, 83.
- (5) (a) Bray, J. W.; Hart, H. R.; Interrante, L. V., Jr.; Jacobs, L. S.; Kasper, J. S.; Watkins, G. D.; Wee, S. H. *Phys. Rev. Lett.* **1975**, *35*, 744. (b) Jacobs, I. S.; Bray, J. W.; Hart, H. R.; Interrante, L. V.; Kasper, J. S.; Watkins, G. D.; Prober, D. E.; Bonner, J. C. *Phys. Rev. B* **1976**, *14*, 3036. (c) Lovett, B. W.; Blundell, S. J.; Pratt, F. L.; Jestadt, T.; Hayes, W.; Tagaki, S.; Kurmoo, M. *Phys. Rev. B* **2000**, *61*, 12241. (d) Huizinga, S.; Kommandeur, J.; Sawatzky, G. A.; Thole, B. T.; Kopinga, K.; de Jonge, W. J. M.; Roos, J. *Phys. Rev. B* **1979**, *19*, 4723. (e) Obertelli, S. D.; Friend, R. H.; Talham, D. R.; Kurmoo, M.; Day, P. J. *Phys.: Condens. Matter* **1989**, *1*, 5671. (f) Liu, Q.; Ravy, S.; Pouget, J. P.; Coulon, C.; Bourbonnais, C. *Synth. Met.* **1993**, *55–57*, 1840. (g) Mukai, K.; Wada, N.; Jamali, J. B.; Achiwa, N.; Narumi, Y.; Kindo, K.; Kobayashi, T.; Amaya, K. *Chem. Phys. Lett.* **1996**, *257*, 538.
- (6) (a) Coomber, A. T.; Beljonne, D.; Friend, R. H.; Brédas, J. L.; Charlton, A.; Robertson, N.; Underhill, A. E.; Kurmoo, M.; Day, P. *Nature* **1996**, *380*, 144. (b) Nishijo, J.; Ogura, E.; Yamaura, J.; Miyazaki, A.; Enoki, T.; Takano, T.; Kuwatani, Y.; Iyoda, M. *Solid State Commun.* **2000**, *116*, 661. (c) Xie, J. L.; Ren, X. M.; Song, Y.; Zou, Y.; Meng, Q. J. *J. Chem. Soc., Dalton Trans.* **2002**, 2868.
- (7) Bulgarevich, S. B.; Bren, D. V.; Movshovic, D. Y.; Finocchiaro, P.; Failla, S. J. *Mol. Struct.* **1994**, *317*, 147.
- (8) Montaudo, G.; Caccamese, S.; Finocchiaro, P. *J. Am. Chem. Soc.* **1971**, *93*, 4202.
- (9) (a) Ren, X. M.; Meng, Q. J.; Song, Y.; Lu, C. S.; Hu, C. J.; Chen, X. Y. *Inorg. Chem.* **2002**, *41*, 5686. (b) Xie, J. L.; Ren, X. M.; Song, Y.; Zheng, W. W.; Liu, W. L.; He, C.; Meng, Q. J. *Chem. Commun.* **2002**, 2346. (c) Xie, J. L.; Ren, X. M.; He, C.; Gao, Z. M.; Song, Y.; Meng, Q. J.; Kremer, R. K. *Chem. Phys. Lett.* **2003**, *369*, 41. (d) Ren, X. M.; Okudera, H.; Kremer, R. K.; Song, Y.; He, C.; Meng, Q. J.; Wu, P. H. *Inorg. Chem.* **2004**, *43*, 2569. (e) Ni, C. L.; Dang, D. B.; Song, Y.; Gao, S.; Li, Y. Z.; Ni, Z. P.; Tian, Z. F.; Wen, L. L.; Meng, Q. J. *Chem. Phys. Lett.* **2004**, *396*, 353. (f) Ni, C. L.; Dang, D. B.; Li, Y. Z.; Yuan, Z. R.; Ni, Z. P.; Tian, Z. F.; Meng, Q. J. *Inorg. Chem. Commun.* **2004**, *7*, 1034. (g) Ni, C. L.; Li, Y. Z.; Dang, D. B.; Ni, Z. P.; Tian, Z. F.; Yuan, Z. R.; Meng, Q. J. *Inorg. Chem. Commun.* **2005**, *8*, 105. (h) Ni, C. N.; Dang, D. B.; Li, Y. Z.; Gao, S.; Ni, Z. P.; Tian, Z. F.; Meng, Q. J. *J. Solid State Chem.* **2005**, *178*, 100. (i) Dang, D. B.; Ni, C. L.; Bai, Y.; Tian, Z. F.; Ni, Z. P.; Wen, L. L.; Meng, Q. J.; Gao, S. *Chem. Lett.* **2005**, *34*, 680.
- (10) Davison, A.; Holm, H. R. *Inorg. Synth.* **1967**, *10*, 8.
- (11) Sheldrick, G. M. *SHELXL-97*, program for the refinement of crystal structure; University of Göttingen: Göttingen, Germany, 1997.
- (12) (a) Hoffmann, R. J. *Chem. Phys.* **1963**, *39*, 1397. (b) Dai, D.; Ren, J.; Liang, W.; Whangbo, M.-H. *CAESAR2* and *SAMOA* (<http://chvaw-w.chem.ncsu.edu>).
- (13) Clementi, E.; Roetti, C. *Atomic Data Nuclear Data Tables* **1974**, *14*, 177.
- (14) Notes: In fact, the Ni(1) atom lies on a general point position, and the two neighboring Ni(1)ⁱ and Ni(1)ⁱⁱ atoms in a stack are generated by the symmetric transforms, where $i = -0.5 + x, 0.5 - y, z$ and $ii = 0.5 + x, 0.5 - y, z$. Defining the fractional coordinates of Ni(1) as (x, y, z) , the coordinates of the two neighbors, $(0.5 + x, 0.5 - y, z)$ of Ni(1)ⁱⁱ and $(-0.5 + x, 0.5 - y, z)$ of Ni(1)ⁱ, are deduced according to the crystal data. Therefore, the Ni(1) ··· Ni(1)ⁱⁱ and Ni(1) ··· Ni(1)ⁱ distances are equal to the moduli of the corresponding vectors of $(0.5, 0.5 - 2y, 0)$ and $(-0.5, 0.5 - 2y, 0)$, respectively, which coincide on the XY-plane of the crystallographic coordinate system. The two-dimensional coordinate system ($X-O-Y$) is orthogonal in the monoclinic system; accordingly, the lengths of the vectors should be given by $|\text{Ni}(1) \cdots \text{Ni}(1)^{ii}| = |(0.5, 0.5 - 2y, 0)| = \{0.5^2 + (0.5 - 2y)^2 + 0^2\}^{1/2}$ and $|\text{Ni}(1) \cdots \text{Ni}(1)^i| = |(-0.5, 0.5 - 2y, 0)| = \{(-0.5)^2 + (0.5 - 2y)^2 + 0^2\}^{1/2} = \{0.5^2 + (0.5 - 2y)^2 + 0^2\}^{1/2}$, so that $|\text{Ni}(1) \cdots \text{Ni}(1)^i| = |\text{Ni}(1) \cdots \text{Ni}(1)^{ii}|$. In other words, the interatomic distances of Ni(1) ··· Ni(1)ⁱ and Ni(1) ··· Ni(1)ⁱⁱ are identical.
- (15) Forrester, J. D.; Zalkin, A.; Templeton, D. H. *Inorg. Chem.* **1964**, *3*, 1507.
- (16) Saito, K.; Massalska-Arodz, M.; Ikeuchi, S.; Maekawa, M.; Sciesinski, J.; Sciesinska, E.; Mayer, J.; Wasutynski, T.; Sorai, M. *J. Phys. Chem. B* **2004**, *108*, 5785.
- (17) Fujita, W.; Awaga, K.; Nakazawa, Y.; Saito, K.; Sorai, M. *Chem. Phys. Lett.* **2002**, *352*, 348.
- (18) Bhatia, S. N.; O'Connor, C. J.; Carlin, R. L.; Algra, H. A.; De Jongh, L. J. *Chem. Phys. Lett.* **1977**, *50*, 353.
- (19) Whangbo, M.-H.; Koo, H.-J.; Dai, D. J. *Solid State Chem.* **2003**, *176*, 417 and references therein.
- (20) Whangbo, M.-H.; Dai, D.; Koo, H.-J. *Dalton. Trans.* **2004**, 3019.
- (21) (a) Bonner, J. C.; Fisher, M. E. *Phys. Rev. A* **1964**, *135* (3A), A640. (b) Hatfield, W. E. *J. Appl. Phys.* **1981**, *52*, 1985.
- (22) Ren, X. M.; Kremer, R. K.; Meng, Q. J. *J. Magn. Magn. Mater.* **2004**, *272–276*, 924.
- (23) Isett, L. C.; Rosso, D. M.; Bottger, G. L. *Phys. Rev. B* **1980**, *22*, 4739.